Metabolism Clinical and Experimental 100 (2019) 153955

Contents lists available at ScienceDirect

Metabolism Clinical and Experimental

journal homepage: www.metabolismjournal.com

Basic Science

Adaptor protein APPL1 coordinates HDAC3 to modulate brown adipose tissue thermogenesis in mice

Linling Fan [a,1], Hongying Ye [a,1], Yun Wan [a], Lang Qin [a], Lu Zhu [a], Jing Su [a], Xiaoming Zhu [a], Lv Zhang [a], Qing Miao [a], Qiongyue Zhang [a], Zhaoyun Zhang [a], Aimin Xu [b], Yiming Li [a], Xi Li [c,*], Yi Wang [a,**]

[a] Department of Endocrinology and Metabolism, Huashan Hospital, Fudan University, Shanghai, China
[b] Department of Medicine, the University of Hong Kong, Hong Kong
[c] Institute of Life Sciences, Chongqing Medical University, China

ARTICLE INFO

Article history:
Received 13 May 2019
Accepted 31 July 2019

Keywords:
Brown adipose tissue
Obesity
APPL1
HDAC3

ABSTRACT

Objectives: The activation of brown adipose tissue (BAT) is considered as a promising therapeutic target for obesity. APPL1 (Adaptor protein containing the Pleckstrin homology domain, Phosphotyrosine binding domain and Leucine zipper motif) is an intracellular adaptor protein and its genetic variation is correlated with BMI and body fat distribution in diabetic patients. However, little is known about the roles of APPL1 in BAT thermogenesis.
Materials/methods: In this study, adipose tissue specific knockout (ASKO) mice were generated to evaluate APPL1's role in BAT thermogenesis in vivo, and possible signaling pathways were further explored in cultured brown adipocytes.
Results: After high fat diet challenge, APPL1 ASKO mice developed more severe obesity, glucose intolerance and insulin resistance compared with control mice. Metabolic cage study showed that APPL1 deficiency impaired energy expenditure and adaptive thermogenesis in ASKO mice. PET-CT analysis showed decreased standardized uptake value (SUV) in the inter-scapular region which indicated impaired BAT activity in ASKO mice. Further study showed deletion of APPL1 attenuated brown fat specific gene expression, such as UCP1 and PGC1α in both BAT and brown adipocytes. In cultured brown adipocytes, upon cAMP stimulation, APPL1 shuttled from cytosol to nuclei. Co-IP and ChIP study showed that APPL1 could directly interact with histone deacetylase 3 (HDAC3) to mediate chromatin remodeling and UCP1 gene expression.
Conclusions: Our data demonstrated the essential role of APPL1 in regulating brown adipocytes thermogenesis via interaction with HDAC3, which may have potential therapeutic implications for treatment of obesity.

1. Introduction

Obesity develops when energy intake exceeds energy expenditure [1]. Therefore, increasing energy expenditure is considered as the promising therapeutic target for obesity. In contrast to white adipose tissue (WAT) that stores energy in the form of triglycerides, brown adipose tissue (BAT) dissipates energy by producing heat to maintain body temperature, by burning glucose and fatty acids in a process called adaptive thermogenesis [2]. BAT is enriched with mitochondria whose inner membrane harbors uncoupling protein 1 (UCP1) that uncouples oxidative respiration from ATP synthesis. It is well established that BAT can be activated in response to cold exposure or by activation of β adrenergic receptors. Moreover, activation of BAT or increasing its mass has been associated with lower body weight and improved glucose and lipid homeostasis [3]. Although much is known about brown adipose commitment and differentiation [4], the detailed transcriptional mechanisms that involved in BAT activation remain unclear [5].

Abbreviations: BAT, brown adipose tissue; WAT, white adipose tissue; APPL1, Adaptor protein containing the Pleckstrin homology domain, Phosphotyrosine binding domain and Leucine zipper motif; ASKO, adipose tissue specific knockout; SUV, standardized uptake value; UCP1, uncoupling protein 1; HATs, histone acetyltransferases; HDACs, histone deacetylases; PGC1α, peroxisome proliferator-activated receptor γ coactivator 1; BAR, N-terminal Bin1/amphiphysin/rvs 167; PH, Pleckstrin homology; BPP, region between PH and PTB; PTB, Phosphotyrosine binding; WT, littermate controls; SCD, standard chow die; HFD, high fat diet; iWAT, inguinal WAT; eWAT, epididymal WAT; TG, triglyceride; TC, total cholesterol; HDL-C, high density lipoprotein cholesterol; AST, aspartate aminotransferase; ALT, alanine aminotransferase; IPGTT, intra-peritoneal glucose tolerance test; IPITT, intra-peritoneal insulin tolerance test; HE, hematoxylin and eosin; SVF, stromal vascular fraction; SEM, standard error of the mean; RER, respiratory exchange ratio; 18F-FDG, 18F-fluorodeoxyglucose; HOMA-IR, insulin resistance index; mtDNA, mitochondrial DNA; co-IP, co-immunoprecipitated; ChIP, chromatin immunoprecipitation; H3K27ac, acetylation of histone 3 lysine 27.

* Corresponding author.
** Correspondence to: Y. Wang, 12 Middle Wulumuqi Road, Department of Endocrinology and Metabolism, Huashan Hospital, Shanghai 200040, China.
E-mail addresses: lixi@shmu.edu.cn (X. Li), aries.520@163.com (Y. Wang).
[1] Linling Fan and Hongying Ye contributed equally to this work.

https://doi.org/10.1016/j.metabol.2019.153955

Accumulating evidence demonstrates the role of histone acetylation in the transcriptional control of BAT gene program and thermogenesis [6]. Histone acetylation is dynamically regulated by histone acetyltransferases (HATs) and deacetylases (HDACs). They are currently classified into four major groups (Class I, II, III, IV) with 18 different subtypes of histone deacetylase [7]. Down-regulation of HDACs stimulates adipocyte differentiation in culture [8]. Treatment of obese mice with Class I HDAC inhibitors can induce peroxisome proliferator-activated receptor γ coactivator 1 (PGC1α), increase mitochondrial biogenesis, enhance oxidative metabolism, increase BAT mass and WAT browning. Furthermore, inhibition of HDAC3 may account for the beneficial effect of the Class I HDAC inhibitors [9]. However, another study reported HDAC1 was a negative regulator of BAT thermogenic program [10]. In addition, the specific mechanism determining how HDACs are involved in the regulation of BAT-specific genes is still unclear. Previous studies suggested β3-adrenergic stimulation in cultured brown adipocytes lead to increased acetylation of H3K27, followed by demethylation of H3K27me3, which allowed transcription [10].

APPL1 consists of the N-terminal Bin1/amphiphysin/rvs 167(BAR) domain (identified as the leucine zipper), followed by a Pleckstrin homology (PH) domain, a region between PH and PTB (BPP) domain (375–499 amino acid), a Phosphotyrosine binding (PTB) domain, and a CC domain at the C-terminus [11,12], an intracellular adaptor protein in the signal transduction with insulin and adiponectin. APPL1 integrates multiple signals through its domains to mediate protein and lipid interactions [11,13]. A study about the single nucleotide polymorphism in patients with type 2 diabetes found that the APPL1 gene polymorphism is associated with body mass index and body fat distribution [14], suggesting that APPL1 is involved in the regulation of obesity and energy metabolism. Diet-induced obese mice and Zucker diabetic fatty rats have reduced expression of APPL1 in adipose, liver, skeletal muscle, and vascular tissues [15–17]. Besides, APPL1 in the cytoplasm could shuttle into the nucleus and mediate chromatin remodeling and gene transcription. The epidermal growth factor treatment can stimulate APPL1 to transfer from cytoplasm into nucleus and interact with nucleosome remodeling and histone deacetylase multiprotein complex NuRD/MeCP1, an established regulator of chromatin structure and gene expression. Other studies reported that APPL1 can directly interact with HDAC3 and mediate the function of HDAC3 [18,19].

Although previous findings suggest a possible role of APPL1 in mediating thermogenesis in adipose tissues, its physiological function in the adipose tissues has not been explored. In this study, we investigated the critical role of APPL1 in the thermogenesis in brown fat using the adipose tissue specific knockout (ASKO) mice and also determined the molecular basis whereby APPL1 modulates HDAC3 to regulate the relevant genes expression in cultured adipocytes. Our data demonstrated APPL1 regulated brown adipocytes thermogenesis via interaction with HDAC3, which may have potential therapeutic implications for treatment of obesity.

2. Materials and methods

2.1. Chemicals and antibodies

The antibodies used for immunoblotting and immunoprecipitation included anti-UCP1 (ab155117; Abcam, Cambridge, United Kingdom), anti-PGC1α (Ab54481; Abcam), anti-HDAC3 (ab7030; Abcam), anti-Acetyl-Histone H3 (K27) (ab4729; Abcam), anti-APPL1 (no.11130; AIS, Hong Kong, China), anti-β-actin (HRP-60008; Proteintech, Chicago, IL), anti-HA Tag (E022180-01, E022010-01; EarthOx, San Francisco, CA), anti-Flag Tag (AT0022; CMCTAG, Milwaukee, WI), anti-Histone H3 (CY5879; Abways, Shanghai, China), anti-Normal Rabbit IgG (no.2729; Cell Signaling Technology, San Antonio, TX), anti-HDAC3 (no.3949; Cell Signaling Technology) and anti-IgG (no.5873; Cell Signaling Technology). All of the other chemicals were purchased from Sigma Chemical/Sigma-Aldrich (St. Louis, MO), Merck-Millipore (Billerica; MA) and Beyotime (Shanghai, China), unless otherwise specified.

2.2. Generation of adipose-specific APPL1 conditional KO mice

The APPL1 flox/flox mice (C57BL/6 background) and the aP2-Cre transgenic mice (C57BL/6 background) (obtained from Shanghai Biomodel Organism Science & Technology Development Co. Shanghai, China) were crossed to generate APPL1 adipose tissue specific knockout mice (ASKO) and littermate controls (WT). Mice divided into groups (3 to 5 animals per cage) were housed at 21 °C ± 1 °C, in 55% ± 15% relative humidity, and under a 12-hour light/dark cycle and fed on a standard laboratory chow diet (SCD) or high-fat diet (HFD) (20% kcal protein, 60% kcal fat, and 20% kcal carbohydrates, Research Diets, New Brunswick, NJ). Animal care procedures were approved by the Animal Care and Use Committee of the Fudan University Shanghai Medical College and followed the National Institute of Health guidelines on the care and use of animals.

2.3. Measurement of body weight, food intake and feeding efficiency

The body weight was measured once a week from the age of 8 weeks both in SCD group and HFD group. Daily food intake was measured in mice that were fed on SCD and HFD by metabolic cage (Columbus Instruments). Food intake normalized by body weight of the mice was represented as feeding efficiency.

2.4. Intraperitoneal glucose tolerance test, insulin tolerance test

For GTT, mice were fasted overnight and were given 20% glucose saline solution (2 g glucose/kg body weight) via intra-peritoneal (i.p.) injection. The glucose concentrations were measured using a glucometer (YUYUE 580, China) in blood collected by venous bleeding from the tail vein at 0, 15, 30, 60, 90, 120 min after glucose administration. The insulin concentrations were measured using an ultra-sensitive mouse insulin ELISA kit (Crystal Chem, USA) in blood collected from the eye vein at 0, 5, 10, 30, 60 min after glucose administration. For ITT, mice were fasted for 6 h and were given recombinant human insulin (Novo Nordisk Danish) (1.5 U/kg) via i.p. injection. The glucose concentrations were measured at 0, 15, 30, 60, 90, 120 min after insulin administration.

2.5. Indirect calorimetry and physical activity

18-week-old mice fed on HFD were housed and monitored individually in a metabolic cage (Columbus Instruments) with free access to regular HFD and drinking water for 72 h. Each cage was monitored for metabolic parameters (including oxygen consumption and carbon dioxide production) at 25-min intervals throughout the 72 h period. Parameters of oxygen consumption ($mL \cdot kg^{-1} \cdot h^{-1}$), carbon dioxide production ($mL \cdot kg^{-1} \cdot h^{-1}$), and RER (CO2/VO2) were calculated for each mouse divided by its body weight. Heat production (energy expenditure) was calculated as described previously [20]. Voluntary activity was derived from the x,y,z-axis beams, which were monitored every 15 min.

2.6. Body fat measurement

Body fat mass and lean mass were measured using a nuclear magnetic resonance instrument (minispec Body Composition Analyzer; Bruker, Billerica, MA). Mice were then euthanized with 10% chloral hydrate water solution and interscapular (BAT), the subcutaneous (inguinal WAT) and visceral (epididymal WAT) fat pads were dissected and their weights were recorded.

2.7. Determination of lipid concentration

Blood samples were centrifuged at 2000*g* for 20 min to obtain serum. Triglyceride (TG), total cholesterol (TC), high density lipoprotein cholesterol (HDL-C), aspartate aminotransferase (AST), and alanine aminotransferase (ALT) levels were analyzed by kits, respectively (BIOTNT, China). The TG content in liver was measured by triglyceride assay kit (A110-1, Nanjing Jiancheng Bioengineering Institute).

2.8. Micro PET/CT

PET-CT imaging was performed at the Micro PET-CT center of the Affiliated Tumor Hospital of Fudan University. Mice were allowed to fast overnight before the experiment. After injecting the 150 μCi 18F-FDG for 60 min, anesthesia induction was performed using isoflurane gas anesthesia system (AS-1-000-1, Summit) (the isoflurane concentration was 2% and the oxygen flow rate was 2 L/min). Inveon PET/CT (Siemens Healthcare, Germany) was used for the scanning process. A 10 min CT X-ray for attenuation correction was scanned with a power of 80 kV and 500 μA and an exposure time of 1100 ms before the PET scan. Ten-minute static PET scans were performed in the same region, and the images were reconstructed of the regions of interest (ROIS). The tracer uptake was measured using the software of Inveon Research Workplace (IRW) 3.0. Individual quantification of the 18F-FDG uptake in each of the ROIs was calculated. The data for the accumulation of 18F-FDG on micro PET images were expressed as the standard uptake values (SUV), which were determined by dividing the relevant ROI concentration by the ratio of the injected activity to the body weight.

2.9. Cold exposure test

Mice of 18-week-age were placed for 4 h in a room with a temperature of 4–8 °C without access to food or water. Body temperature was recorded once per 20 min with a rectal probe connected to a digital thermometer.

2.10. Histology and immunohistochemistry

Adipose tissues fixed in 4% paraformaldehyde were sectioned after being paraffin embedded. Multiple sections were prepared and stained with hematoxylin and eosin (HE) for general morphological observations. Immunohistochemistry staining was performed according to the standard protocol using UCP1 antibody, incubating overnight in a humidified chamber at 4 °C. The secondary antibody for immunohistochemistry staining was purchased from Gene Tech Company limited (Shanghai).

2.11. Cell culture and differentiation

The HEK293T cells were propagated in Dulbecco's modified Eagle medium (DMEM) containing 10% fetal bovine serum (FBS). HA-HDAC1–3 plasmids were generous gifts from professor Qunying Lei (Fudan University). Flag-APPPL1 plasmid was constructed using a standard PCR-based cloning technique from cDNA templates with different primer sets containing Flag sequences. The PCR products of target genes were cloned into the vector pcDNA3.1 and verified by DNA sequencing. The restriction enzymes sites were *Xho* I/Hind III. Primer sequences of Flag-APPL1 were as follows: F: 5′ CCTAAGCTTATGGATTACAAGGATGA CGACGATAAG CCGGGGATCGACAAGCTGCCCATCGAGGA GACG 3′ and R: 5′ CGCCTCGAGTCATTATGCTTCTGATTCTCTCTTCTT 3′. Plasmid transfections were conducted with Lipofectamine 2000 (Invitrogen) according to the manufacturer's instructions.

Primary interscapular brown fat stromal vascular fraction (SVF) was obtained by collagenase I digestion from 4- to 6-week-old WT or ASKO male mice, according to the published methods [20]. SVF cells were maintained in DMEM (F12) with 10% FBS at 37 °C in a 5% CO_2 cell culture incubator. Adipocyte differentiation was supplemented with isobutyl methylxanthine (0.5 mM), indomethacin (125 μM), dexamethasone (2 μg/mL), insulin (5 μg/mL), and triiodothyronine (1 nM) with rosiglitazone (1 μM) 10% FBS. After 48 h, the medium was removed and replaced by another medium containing 10% FBS, insulin (5 μg/mL), and triiodothyronine (1 nM) with rosiglitazone (1 μM). Cells were harvested at day 8–10 days after differentiating into adipocytes.

2.12. Transmission electron microscopy

BAT sections were fixed in 2.5% (vol/vol) glutaraldehyde including 0.1 M phosphate buffer, PH7.2 for 12 h at 4 °C. The sections were then post-fixed in 1% osmium tetroxide, dehydrated in ascending gradations of ethanol and embedded in pure acetone and embedded liquid. The sections then were put into 37 °C oven overnight. Ultra-thin sections (60–80 nm) were cut and stained with lead citrate before being examined on JEOL JEM-1230 (80 kV) transmission electron microscope.

2.13. Mitochondrial DNA content quantification by quantitative real-time PCR

Genomic DNA was isolated from BAT from WT and ASKO mice, respectively. The tissues were homogenized and digested with proteinase K at 55 °C overnight in a lysis buffer for DNA extraction by a conventional phenol-chloroform method. The data are expressed as mtDNA-specific 16S ribosomal RNA normalized to the nuclear specific gene *Sun1*. The sequences of the primers used in this study are listed in Table 1.

2.14. Oil Red O staining

Dishes with adipocytes were washed three times with phosphate-buffered saline (PBS) and fixed with 10% formalin for 20 min at room temperature. The cells were washed three times in PBS, stained for 1 h at 37 °C with a filtered Oil Red O working solution (0.5% Oil Red O in isopropyl alcohol), and then washed three times with distilled water and visualized under an inverted microscope.

Table 1
DNA primers for quantitative QPCR.

cDNA	Forward	Reverse
18s	CGCCGCTAGAGGTGAAATTCT	CATTCTTGGCAAATGCTTTCG
UCP1	AGGCTTCCAGTACCATTAGGT	CTGAGTGAGGCAAAGCTGATTT
PGC1α	GTCAACAGCAAAAGCCACAA	TCTGGGGTCAGAGGAAGAGA
DIO2	CAGTGTGGTGCACTGCTCCAATC	TGAACCAAAGTTGACCACCAG
COX8b	TGTGGGGATCTCAGCCATAGT	AGTGGGCTAAGACCCATCCTG
CIDEA	ATCACAACTGGCCTGGTTACG	TACTACCCGGTGTCCATTTCT
ELOVL3	TCCGCGTTCTCATGTAGGTCT	GGACCTGATGCAACCCTATGA
ATPsyn	GGTTCATCCTGCCAGAGACTA	AATCCCTCATCGAACTGGACG
MACD	CAACACTCGAAAGCGGCTCA	ACTTGCGGGCAGTTGCTTG
CPT1b	GCACACCAGGCAGTAGCTTT	CAGGAGTTGATTCCAGACAGGTA
PRDM16	CAGCACGGTGAAGCCATTC	GCGTGCATCCGCTTGTG
TFAM	GGAATGTGGAGCGTGCTAAAA	ACAAGACTGATAGACGAGGGG
NRF1	AGCACGGAGTGACCCAAAC	TGTACGTGGCTACATGGACCT
COX7a1	CAGCGTCATGGTCAGTCTGT	AGAAAACCGTGTGGCAGAGA
Cytoc	CCAAATCTCCACGGTCTGTTC	ATCAGGGTATCCTCTCCCCAG
422ap2	CACCGCAGACGACAGGAAG	GCACCTGCACCAGGGC
PPARγ	GACCACTCGCATTCCTTT	GGCATTGTGAGACATCCC
PPARα	AGAGCCCCATCTGTCCTCTC	ACTGGTAGTCTGCAAAACCAAA
C/EBPβ	GCACACCAGGCAGTAGCTTT	CAGGAGTTGATTCCAGACAGGTA
Mito-SUN1	GACCCTGTATACTTTCTGTTGG	AACAGGTAAGTCTGGAAAAAGG
Mito-16sRNA	CCGCAAGGGAAAGATGAAAGAC	TCGTTTGGTTTCGGGGTTTC
NDUFB9	GGTGCGTCCAGAGAGACAAA	ATCACCTTCCTTTCGGGCAG
COXII	TCTCCCCTCTCTACGCATTCTA	ACGGATTGGAAGTTCTATTGGC
COXIV	ATGTCACGATGCTGTCTGCC	GTGCCCCTGTTCATCTCGGC
COX8H	AGGAGTGCGACCCCGAGAATC	GGCTAAGACCCATCCTGCTGG
ATP5B	GCAAGGCAGGGACAGCAGA	CCCAAGGTCTCAGGACCAACA
ERRα	GGAGGACGGCAGAAGTACAAA	GCGACACCAGAGCGTTCAC
ERRγ	TCCCCGACAGTGACATCAAA	GTGTGGAGAAGCCTGGAATA
NRF-2	CCGCTACACCGACTACGATT	ACCTTCATCACCAACCCAAG

2.15. Oxygen consumption in differentiated SVF from BAT

Basal and cAMP-stimulated oxygen consumption was measured with a Clark-type oxygen electrode (Hansatech Instruments Ltd.). In each experiment, differentiated brown adipocytes were added to the oxygen electrode chamber. Basal respiration was measured for 2–4 min. Then, cAMP was added and oxygen consumption monitored for an additional time of 3–5 min. Experiment was repeated for >3 times.

2.16. Immunoprecipitation and immunoblotting

The cells and tissues were lysed on ice in radioimmunoprecipitation assay (RIPA) buffer (1% Triton X-100, 50 mM Tris [pH 7.4], 150 mM NaCl) containing 50 mM NAM and protease inhibitor mixture (Roche). After incubation on ice for 30 min and centrifugation for 10 min at 4 °C. equal volumes of protein were diluted with lysis buffer. For immunoprecipitation, cell lysates were incubated with the indicated antibodies overnight at 4 °C on a rotating wheel and with protein G-agarose beads (Millipore) for another 4 h. The binding complexes were washed four times with RIPA buffer and then subjected to SDS-PAGE. For immunoblotting, equal amounts of protein were separated on SDS-PAGE, blotted onto a polyvinylidene difluoride membrane (Millipore), incubated with primary antibodies. After the priming antibodies were washed, the membranes were incubated with secondary antibodies conjugated with horseradish peroxidase, followed by detection with ECL Western blotting detection solutions.

2.17. Quantitative real-time PCR analysis

The total RNA was prepared with Trizol method (Thermo Fisher Scientific, Waltham, MA) following the manufacturer's instructions. Complementary DNA was prepared from 500 ng of RNA using the Reverse Transcription System (YEASEN, Shanghai, China). Then, 1 μL of diluted complementary DNA was used in a 10 μL PCR reaction with SYBR Green Master Mix (YEASEN, Shanghai, China). PCRs were run in triplicate for each sample and analyzed in a Prism 7500 instrument (Applied Biosystems), with 18s as an endogenous control. Sequences of the primers used in this study were listed in Table 1.

2.18. Chromatin immunoprecipitation

Chromatin immunoprecipitation was performed using a ChIP assay kit (Millipore). For tissue ChIP assays, tissue samples were cut into small pieces and fixed with 1% of formaldehyde. The samples were homogenized in cell lysis buffer using automatic rapid grinding instrument (Shanghai Jingxin Industrial Development Co. Ltd.) to isolate nuclei. The nuclei were resuspended in nuclei lysis buffer and sonicated to shear genomic DNA to an average fragment length of 200–1000 bp with a Cole-Parmer, High Intensity Ultrasonic Processor. Lysates were centrifuged at 4 °C and the supernatants were collected. 5 μL of each sample was removed as the input control. The supernatants underwent overnight immunoprecipitation, elution, reverse cross-linking, and protease K digestion, according to the manufacturer's manual. A mock immunoprecipitation without antibody was also included for each sample. Eluted DNA was analyzed by real-time PCR using SYBR Green quantitative PCR (YEASEN, Shanghai, China). Primer sequences used in this study were as follows: Ucp1 proximal promoter, 5′-CCCACTAGCAGCTC TTTGGA-3′ and 5′-CTGTGGAGCAGCTCAAAGGT-3′; Ucp1 enhancer region, 5′-CTCCTCTACAGCGTCACAGAGG-3′ and 5′-AGTCTGAGGAAAGG GTTGA-3′; Ucp1-2 kb enhancer: 5′-TCACCCTTGACCACACTGAA-3′ and 5′-GTGAGGCTGATATCCCCAGA-3′; Ucp1-5 kb enhancer, 5′-TGCAAC CCCTCACCTTTTAC-3′ and 5′-CTCCTTCCATCATCCCTTCA-3′; Ucp1-6 kb enhancer, 5′-GAAGCAGAGGGCTCACAAAC-3′ and 5′-CCTTGCAGAAA GGGTCAAAA-3′; Ucp1-13 kb enhancer, 5′-GCAACCCTCTCCCATCAGTG-3′ and 5′-GCCTAACACCGTGCTTCTCA-3′.

2.19. Statistical analysis

All experiments were independently repeated at least three times, and data are expressed as the mean ± standard error of the mean. Statistical analyses were completed using a two-tailed unpaired Student *t*-test or 2-way analysis of variance. $P < 0.05$ was considered statistically significant.

3. Results

3.1. Ablation of APPL1 in adipose tissue exacerbates HFD-induced obesity

Because of the hormone fluctuations in female mice, only male ASKO and WT mice were used in the following study. We successfully got the APPL1 ASKO mice via the cre-lox system (sFig. 1). APPL1 ASKO male mice did not differ in their body weights from WT mice on SCD. After HFD challenge, ASKO mice became significantly heavier than WT mice after 5 weeks (Fig. 1A), although their body lengths were unaltered (Fig. 1B). After 9 weeks on HFD, ASKO mice were considered obese, weighing about 41 g, which was >25% than WT mice (Fig. 1A, right). The gross appearance of ASKO mice fed on HFD appeared much fatter than the WT mice (Fig. 1C). There was a statistical difference in the tissue weights of iWAT and eWAT between ASKO and WT mice on HFD (Fig. 1D). Nuclear magnetic resonance analysis revealed that 18-week-old male ASKO mice fed on the HFD had an increase in the whole-body fat content, although their lean mass did not change (Fig. 1E).

3.2. APPL1 deficiency impairs energy expenditure and adaptive thermogenesis

We firstly examined the alteration in daily food intake in ASKO mice. No significant alteration in daily food intake was observed in APPL1 ASKO mice both on the SCD and the HFD (Fig. 2A). The body weight-normalized food intake (feeding efficiency) did not change between ASKO mice and WT mice (Fig. 2A). These data showed APPL1 deficiency did not affect energy intake. Because deletion of APPL1 exacerbated HFD-induced obesity without affecting energy intake, we examined whether the increased adiposity was associated with a decrease in energy expenditure. As a result, we performed direct calorimetric measurements. On HFD, the basal oxygen consumption and carbon dioxide production rates through a 12-h light/dark cycle were substantially decreased in APPL1 ASKO mice relative to those of WT mice (Fig. 2B). The ASKO mice also showed significant decrease in the whole-body energy expenditure (Fig. 2C) but not the respiratory exchange ratio (RER) which reflects the relative use of carbohydrates versus lipids as a source of energy (Fig. 2D). The lower energy expenditure in the ASKO mice was not due to a decrease in physical activity as their movements were similar compared to the WT mice (Fig. 2E). To further examine the differences in energy expenditure among these mice, we performed a cold tolerance test to measure adaptive thermogenesis. During 4 h of exposure to the cold (4–8 °C), body temperature of the APPL1 ASKO mice dropped on SCD. However, body temperature of APPL1 ASKO mice did not show a significant decrease on HFD which was possibly due to the inadequate cold exposure time for the obese mice. It displayed impaired adaptive thermogenesis in ASKO mice (Fig. 2F). These results imply that APPL1 plays an important role in keeping body adaptation to cold exposure by increasing energy expenditure.

In order to examine the activity of BAT, we used micro PET/CT to characterize the 18F-fluorodeoxyglucose (FDG) uptake in the interscapular region of both ASKO and WT mice in vivo. The combination of CT and PET images showed that the standard uptake value (SUV) was lower in the interscapular BAT position of the ASKO mice. The calculation results of the SUV suggested that APPL1 ASKO mice had a lower activity of BAT (Fig. 2G), which induced the impaired adaptive thermogenesis in BAT.

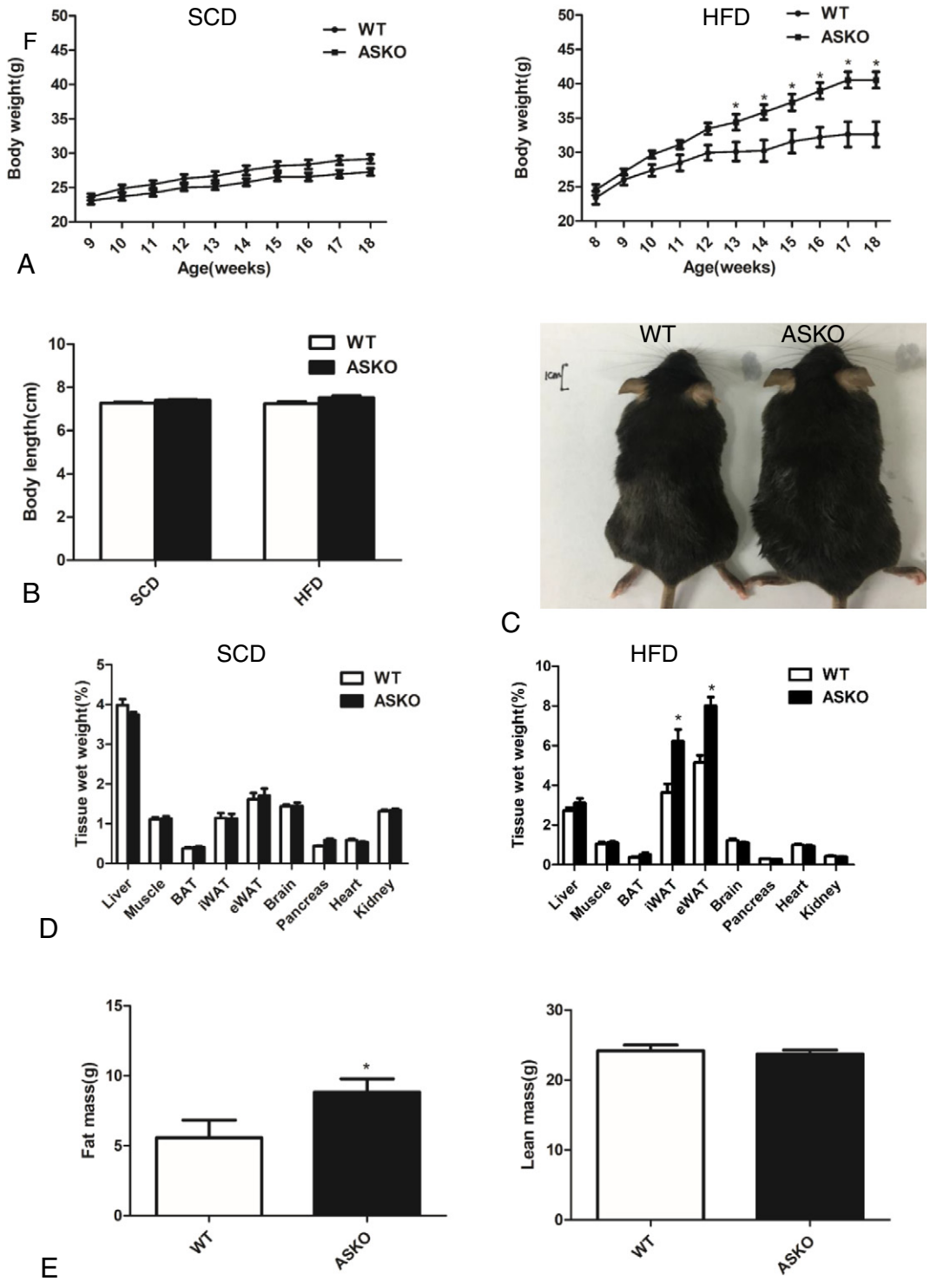

Fig. 1. Ablation of APPL1 in adipose tissue exacerbates HFD-induced obesity. A: Growth curves of male littermates fed on the SCD (left) and HFD (right), ($n = 10$ each group). B: Body length (16-weeks-old male mice). C: Representative images of 18-weeks-old WT (left) and APPL1 ASKO (right) male mice fed on HFD. D: Tissue wet weight (% body weight) of 18-weeks-old WT and APPL ASKO male mice fed on SCD (left) or HFD (right) ($n = 10$ each group). E: Fat mass weight and lean mass weight of male littermate ($n = 10$ each group on HFD). Data are represented as mean ± standard error of the mean (SEM), and significant differences compared with controls are indicated by $^*P < 0.05$.

3.3. APPL1 deficiency leads to glucose intolerance and insulin resistance

To evaluate the impact of adipose-specific KO of APPL1 on glucose metabolism, we examined the blood glucose and insulin levels in APPL1 ASKO mice and WT mice. Comparing the glucose tolerance test responses and the insulin tolerance test responses between APPL1 ASKO and WT mice both on the SCD and HFD, the results showed that ASKO mice had impaired glucose tolerance under glucose challenge and the blood glucose levels were significantly higher compared to WT mice in response to insulin challenge (Fig. 3A, B), which indicated glucose intolerance and insulin resistance in ASKO mice. In glucose tolerance test, more insulin was needed to lower the glucose level in blood in APPL1 ASKO mice and the insulin resistance index (HOMA-IR) was higher in APPL1 ASKO mice (Fig. 3C),

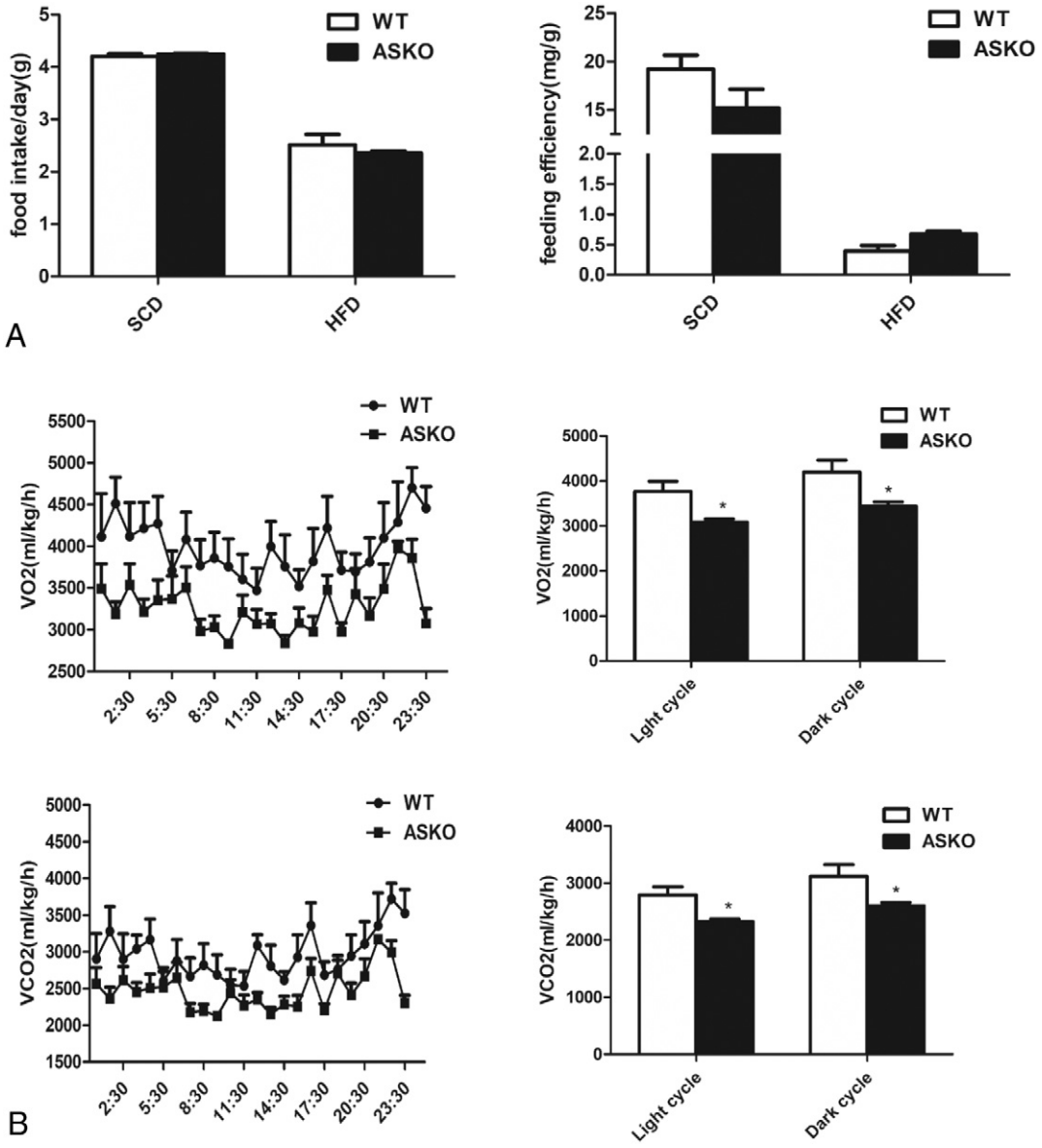

Fig. 2. APPL1 deficiency decreases oxygen consumption and energy expenditure. A: Daily food intake and feeding efficiency (calculated as average change in body weight by average food intake). B: Whole-body oxygen consumption rate (VO2) and carbon dioxide release (VCO2) are measured to evaluate the energy expenditure. C: Heat production expressed as $Kcalh^{-1}$ per littermate was calculated. D: Average RER of each group in a 24 h cycle was calculated by dividing VCO2 by O2 E: Ambulatory activities were measured by activity sensor (beam breaks) both on dark circle and light circle. F: Rectal temperatures of 18-weeks-old WT and APPL1 ASKO male mice fed on SCD or HFD when kept at different time after exposure to cold (4 °C) without food deprivation. G: PET/CT images of WT and ASKO mice after injection of 18F-FDG. The white circles represent the interscapular BAT. The activity of BAT in grams times the mean standard uptake value (SUV). The table (right) shows the SUV ($n = 6$ per genotype on HFD). Data are represented as means ± SEM, and significant differences compared with controls are indicated by $^{*}P < 0.05$, $^{**}P < 0.01$.

which further confirmed that the ASKO mice obtained worse insulin resistance. We also detected the lipid metabolism in ASKO mice and the data showed that fasting TG level in liver and fasting AST in serum increased significantly compared to those in the WT. But there was no significant alteration in fasting ALT, HDL-C, TC and TG serum levels in either genotype (sFig. 2). These data showed that ASKO mice exhibited more severe glucose and lipid metabolism disorders.

3.4. Deletion of APPL1 attenuates brown fat specific gene expression and mitochondria number

Consistent with the increase in body weight, larger multilocular lipid droplets were observed in the BAT, WAT of APPL1 ASKO mice (Fig. 4A, sFig. 3A, D). Moreover, Immunohistochemistry and Immunoblotting analysis showed that BAT from APPL1 ASKO mice on HFD had lower expression level of specific-brown gene UCP1 (Fig. 4B, C). Consistently, the expressions of the mRNAs relevant to BAT markers (UCP1, PGC1α, Dio2, Elovl3, Cidea, PRDM16), mitochondrial related genes (NDUFB9, Cox7a1, Cox8b, COXII, COXIV, COX8H, Cytoc, ATP5B, ERRα, ERRγ, NRF1, NRF-2, Tfam), transcription factors (422ap2, PPARγ, PPARα) and β-oxidation-related genes (ATP synthase, MACD, CPT1B) were decreased markedly in BAT from ASKO mice on HFD (Fig. 4D). However, there was no significant difference in thermogenic gene expressions in WAT, possibly due to the thermogenic gene expressions already being low in WAT at a basal level (sFig. 3B, C, E, F). As shown in Fig. 4E, the number of mitochondria was decreased as observed by means of transmission electronic microscopy in APPL1 ASKO on HFD and quantified by mitochondrial DNA (mtDNA) copy number.

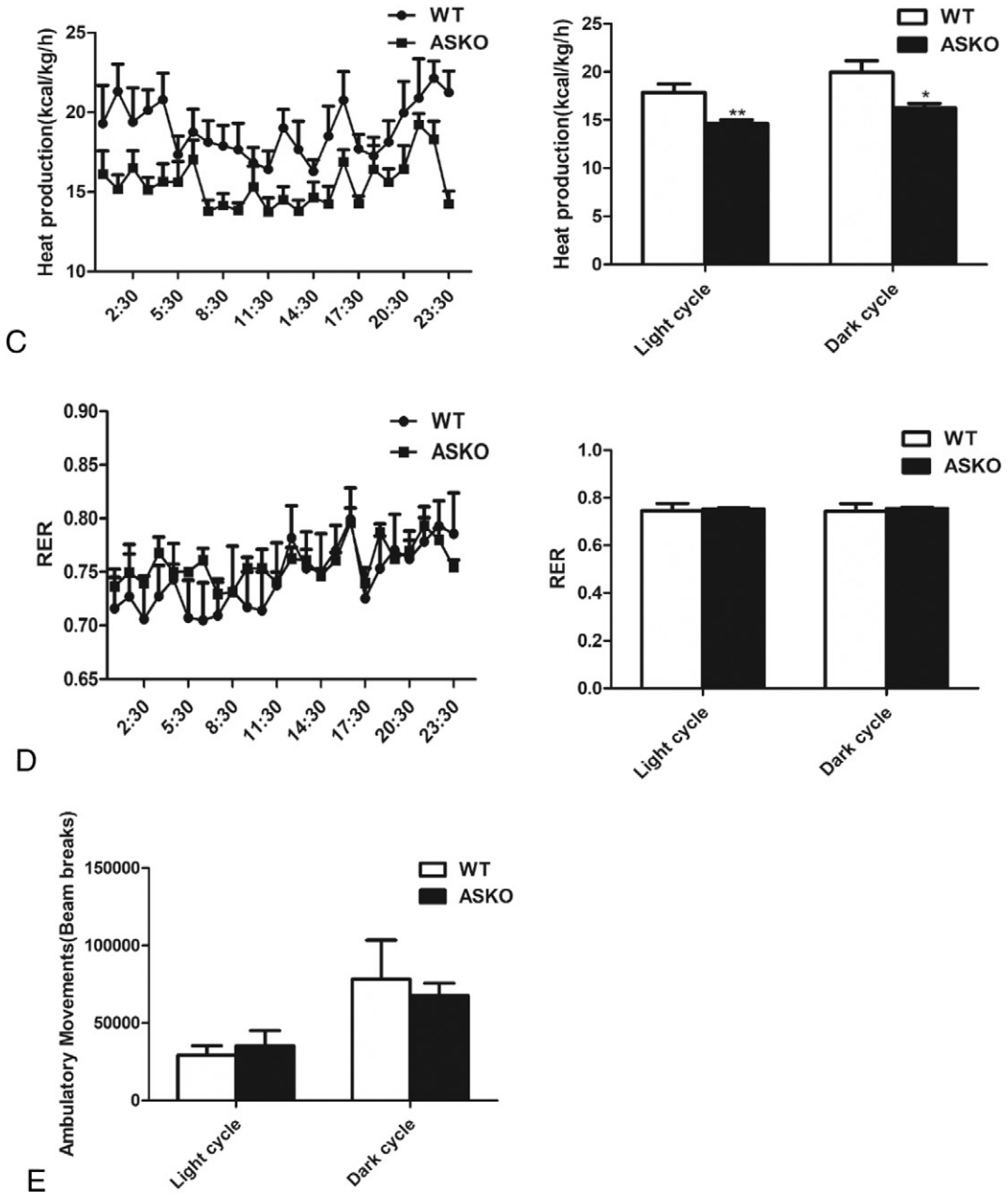

Fig. 2 (*continued*).

3.5. APPL1-deficiency results in decreased thermogenic gene expression in SVF from BAT

To investigate the direct effect of APPL1 on brown adipocytes, fractionated and differentiated brown fat SVF from 4- to 6-week-old male ASKO and WT mice were tested. The protein level of UCP1 was down regulated evidently in the differentiated SVF from the ASKO mice (Fig. 5A). We also observed a marked decline in BAT marker genes (UCP1 and PGC1α), transcription factors (C/EBPβ and PPARγ) at the mRNA level (Fig. 5B). As shown in Fig. 5C, the differentiated SVF brown adipocytes lacking APPL1 exhibits a statistical decrease in basal oxygen consumption compared to WT. Under cAMP stimulation, the oxygen consumption difference between WT and ASKO brown adipocytes was more significant. Furthermore, we found that SVF from ASKO mice were well-differentiated as that from WT mice via Oil Red O staining test and the expressions of differentiation-related genes did not change (422ap2, PRDM16) (Fig. 5D). These results indicate that APPL1 deficiency in brown adipocyte affected its thermogenesis rather than adipogenesis.

3.6. APPL1 interacts with HDAC3 by nucleus shuttling in adipocytes

Previous findings suggested that APPL1 could modulate gene expression by interacting with histone deacetylase. To further elucidate which HDAC interacts with APPL1, we co-transfected HA-tagged HDAC1–3 respectively and FLAG-tagged APPL1 plasmids into HEK 293T cells. Cell extracts were immunoprecipitated with anti-HA or anti-FLAG beads, and analyzed by Western blotting. As shown in Fig. 6A, APPL1 co-immunoprecipitated (co-IP) with HDAC3 but not HDAC1 and HDAC2. To further confirm the interaction between APPL1 and HDAC3, we directly used BAT extracts to see that APPL1 was immunoprecipitated with HDAC3 (Fig. 6A).

cAMP mimics BAT activation in vitro. Under cAMP stimulation, APPL1 shuttled from cytosol to nucleus. We collected the proteins

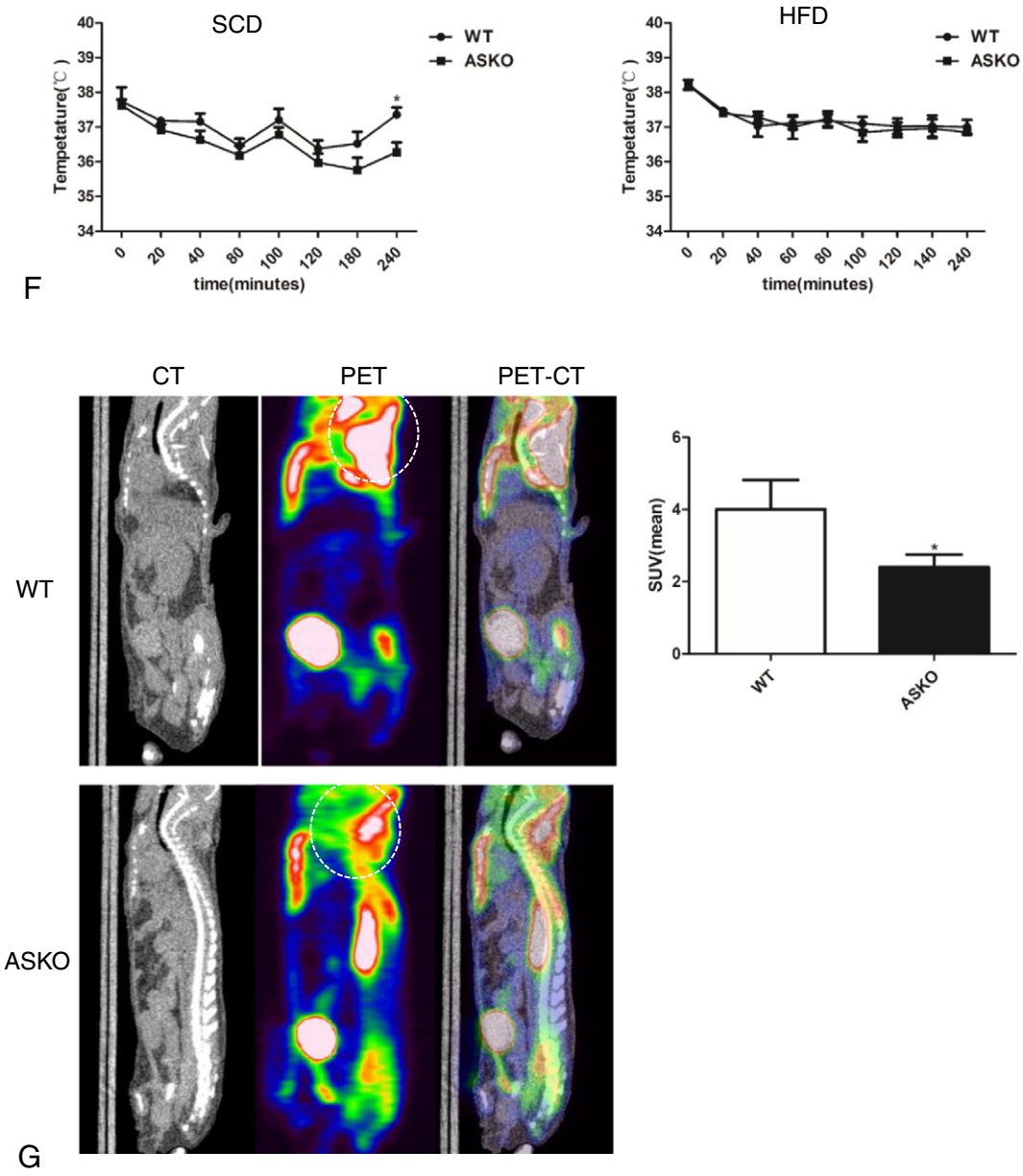

Fig. 2 (*continued*).

from whole cell lysates, cytosolic fractions and nuclear fractions respectively to verify the nuclear translocation of APPL1. The expression of APPL1 was increased in the nucleus and decreased in the cytoplasm, but the total concentration was constant in the whole cells (Fig. 6B). This suggested that APPL1 may modulate brown adipocyte thermogenic gene expression through shuttling between nucleus and cytoplasm.

We therefore examined the binding of APPL1 and HDAC3 at the enhancer and proximal promoter regions of UCP1. As expected, binding of APPL1 and HDAC3 was significantly increased at the enhancer and proximal promoter regions of UCP1 compared to binding of IgG in BAT of mice. Cold exposure leads to a critical increase in APPL1 binding at the enhancer and promoter regions of UCP1. By contrast, cold exposure deceased the binding of HDAC3 to these promoter/enhancer regions. In addition, the binding of HDAC3 was obviously increased in the ASKO mice (Fig. 6C). As has been reported, H3K27 is a special histone site for HDAC3. To further confirm the effect of APPL1 on HDAC3, we use differentiated SVF from ASKO and WT mice, and BAT from ASKO and WT mice. We found that APPL1 overexpression increased the acetylation level of H3K27ac while APPL1 deficiency conversely decreased the acetylation level (Fig. 6D). The results above suggested that APPL1 can shuttle from cytoplasm to nucleus to inhibit the function of HDAC3 to increase the acetylation level of H3K27ac in order to upregulate the expression of BAT marker gene (UCP1).

4. Discussion

BAT activation is considered as a promising therapeutic target for obesity. It is well established that BAT can be activated in response to cold exposure, while the detailed molecular mechanisms of BAT activation need to be further elucidated [5]. In this study, we demonstrated that APPL1 coordinates HDAC3 to modulate adaptive thermogenesis of BAT.

APPL1 integrates multiple signals through its domains to mediate protein and lipid interactions [11,13]. As a critical player in both insulin and adiponectin signaling, APPL1 serves as an important mediator in the cross-talk between these two signaling pathways. Overexpression of

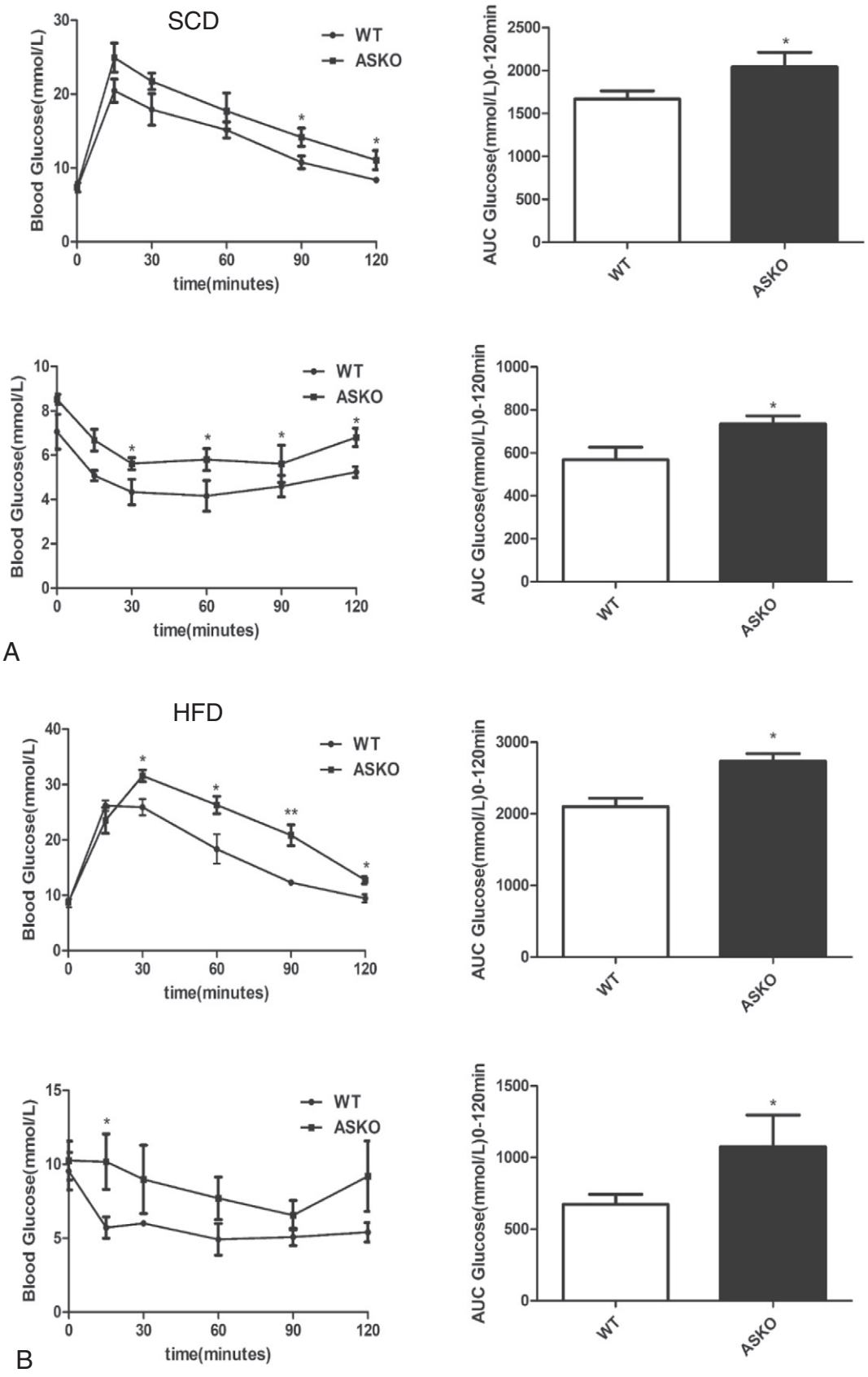

Fig. 3. APPL1 deficiency leads to glucose intolerance and insulin resistance. Blood glucose levels during intraperitoneal glucose tolerance test (IPGTT) and insulin tolerance test (IPITT) for 18-weeks-old male mice on SCD (A) or HFD (B). Representative areas under both GTT and ITT curves are analyzed. C: Plasma insulin levels during IPGTT for 18-weeks-old male mice denied food overnight. HOMA-IR stands for Homeostatic Model Assessment of Insulin Resistance ($n = 5$ mice each group on HFD). Data are represented as means ± SEM, and significant differences compared with controls are indicated by $^{*}P < 0.05$, $^{**}P < 0.01$.

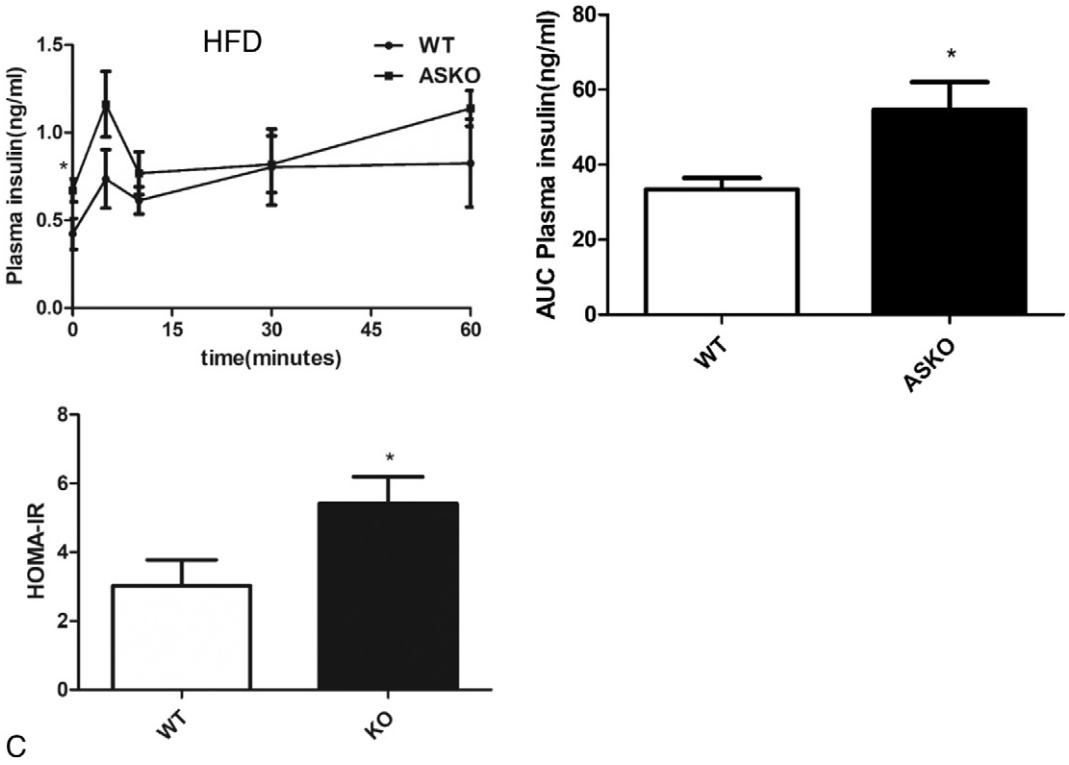

Fig. 3 (*continued*).

APPL1 could suppress hepatic glucose production [21], increase skeletal muscle glucose uptake [22,23] and stimulate insulin secretion in pancreatic islet [24]. A study about the single nucleotide polymorphism in patients with type 2 diabetes found that the APPL1 gene polymorphism is associated with body mass index and body fat distribution [14]. The frequency of G allele was significantly higher in patients with higher waist circumference, suggesting that APPL1 is involved in the regulation of obesity and energy metabolism. It has been documented that APPL1 expression was down regulated in obese mice [16]. In our previous study, we found that APPL1 could counteract obesity induced endothelial dysfunction [25] and general overexpression APPL1 transgenic mice were resistant to high fat diet induced obesity. Cold exposure could enhance APPL1 expression in BAT (data not shown). To elucidate the role of APPL1 in BAT thermogenesis, we generated adipose tissue specific knockout APPL1 mice.

Although Fabp4-Cre transgenic mice have been extensively used to achieve adipocyte-specific deletion, some degree of recombination in other cells and tissues, such as macrophages or endothelial cells, has been reported [26]. In the present work, we did not find significant APPL1 deletion in the bone marrow macrophages, liver, skeletal muscle, pancreas, heart, kidney or brain of ASKO mice (sFig. 1E). Furthermore, previous findings suggested that APPL2, not APPL1, played a dominant role in macrophages [27]. These findings allow us to conclude that the observed phenotypes in male ASKO mice on HFD essentially derived from the deletion of APPL1 in adipocytes.

Deletion of APPL1 in adipose exasperated the detrimental impact of HFD on body weight gain, glucose tolerance, systematic insulin sensitivity, and energy expenditure. Most importantly, this work demonstrates for the first time that APPL1 deficiency impairs energy expenditure and adaptive thermogenesis. In this study, we performed direct calorimetric measurements using metabolic chamber. The ASKO mice showed significant decrease in the whole-body energy expenditure and impaired adaptive thermogenesis. Also, the PET-CT scanning showed lower SUV values in the interscapular BAT position of the APPL1 ASKO mice after cold challenge (Fig. 2G).

Brown adipose tissue activity has been shown to be related to body weight regulation, glucose, and lipid homeostasis in mice [28–30]. Obese humans have reduced BAT compared to those with normal weight [31]. A recent study employing retrospective analysis of FDG-PET/CT scans of 4852 patients showed that BAT-positive patients had lower visceral, subcutaneous and liver fat content [32]. In this study, although body weight did not differ significantly between SCD-fed ASKO and WT mice, ASKO mice were more susceptible to HFD-induced obesity. Obese ASKO mice displayed BAT dysfunction, such as enlarged brown adipocytes, decreased activity of BAT, decreased UCP1 gene and protein expression. ASKO mice showed more severe glucose intolerance and insulin resistance on HFD. In conclusion, APPL1 plays a critical role in regulation of BAT activity to combat obesity and to improve metabolic state in mice.

Although APPL1 was expressed both in WAT and BAT, the expression profile suggested that APPL1 mRNA and protein expression were much higher in BAT than WAT (sFig. 1E). HE staining showed bigger adipocyte size in both iWAT and eWAT from APPL1 ASKO mice compared to WT control (sFig. 3). We also detected UCP1 and PGC1α expression in WAT by western blot, while the protein levels were very low in both ASKO mice and WT control. QPCR showed that thermogenic genes expression was similar between two groups. Therefore, we conclude that deletion of APPL1 has a negligible to mild effect on WAT function. Impaired BAT activation is responsible for the phenotype of ASKO mice.

A series of studies have shown that APPL1 mediates chromatin remodeling and gene transcriptions by nucleus shuttling [11,33–35]. In hela cells, APPL1 binding with the GTPase Rab5 can translocate from the membranes to nucleus, where it interacts with HDACs to mediate gene transcription [11]. Histone deacetylases (HDACs) catalyze the removal of acetyl from the amino terminal lysine residues of core histones, which generally is associated with gene repression. There are four classes of HDACs with different structures and enzymatic functions. Class I HDACs consist of HDAC1, HDAC2, HDAC3, and HDAC8, which are ubiquitously expressed and located

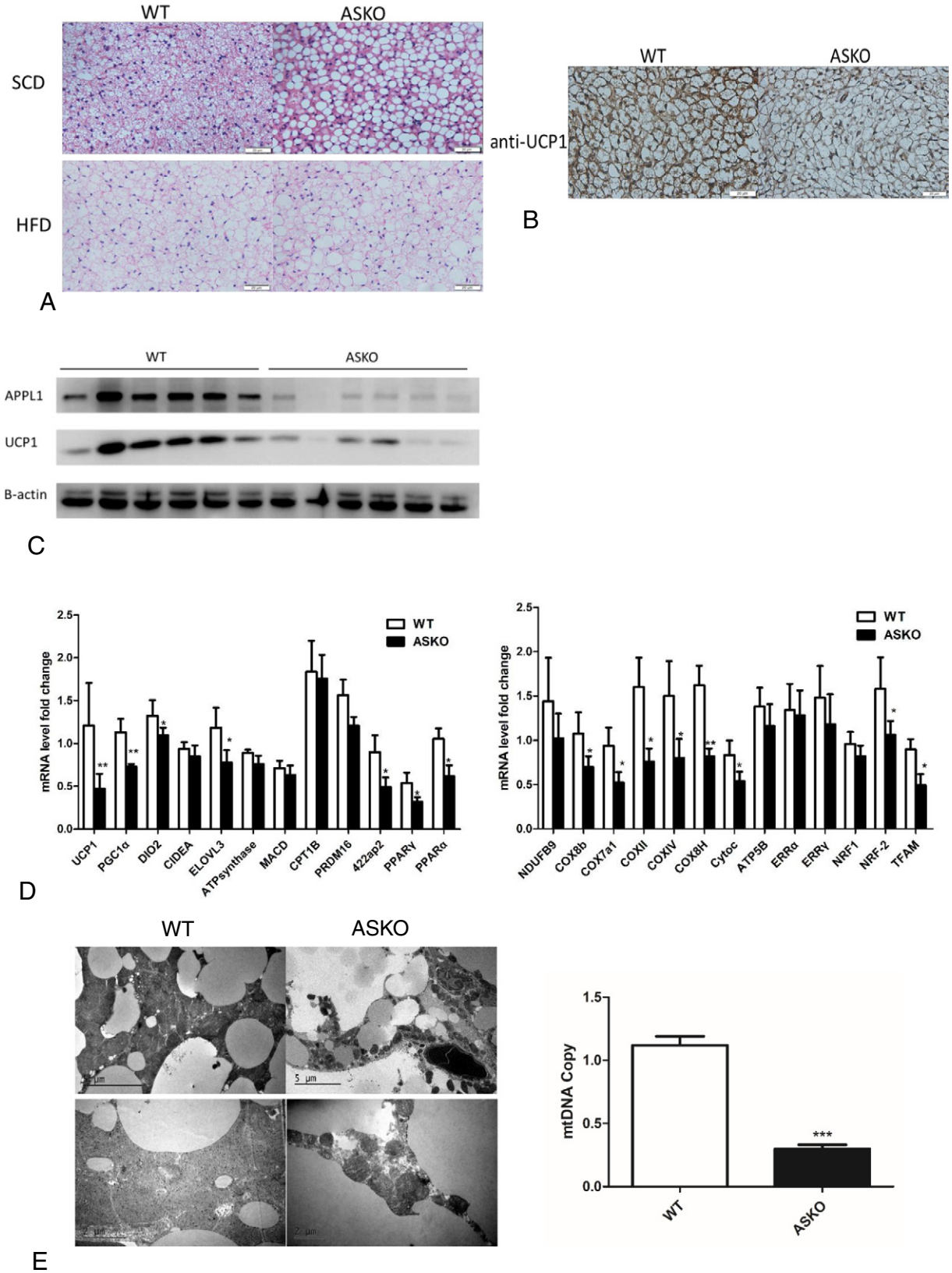

Fig. 4. APPL1 deficiency induces whitening of BAT. A: Representative hematoxylin and eosin (HE) staining per genotype per diet. B: Immunohistochemistry for UCP1 in BAT sections on HFD. Scale bar, 20 μm. C: Western blot shows induction of UCP1 protein expression in BAT of 18-weeks-old WT and APPL1 ASKO male mice fed on HFD. D: Real-time qPCR detects relative mRNA expressions (UCP1, PGC1α, Dio2, Cidea, Elovl3, ATP synthase, MACD, PRDM16, 422ap2, PPARα/γ, NDUFB9, Cox7a1, Cox8b, COXII, COXIV, COX8H, Cytoc, ATP5B, ERRα, ERRγ, NRF1, NRF-2, Tfam) in BAT of 18-weeks-old WT and APPL1 ASKO male mice fed on HFD. E. Electron micrographs of BAT from 18-weeks-old WT and APPL1 ASKO male mice fed on HFD. Scale bar: 5 μm and 2 μm respectively. Mitochondria relative mtDNA copy number in BAT of 18-weeks-old male mice ($n = 10$ each group on HFD). Data are represented as means ± SEM, and significant differences compared with controls are indicated by $^{*}P < 0.05$, $^{**}P < 0.01$ and $^{***}P < 0.001$.

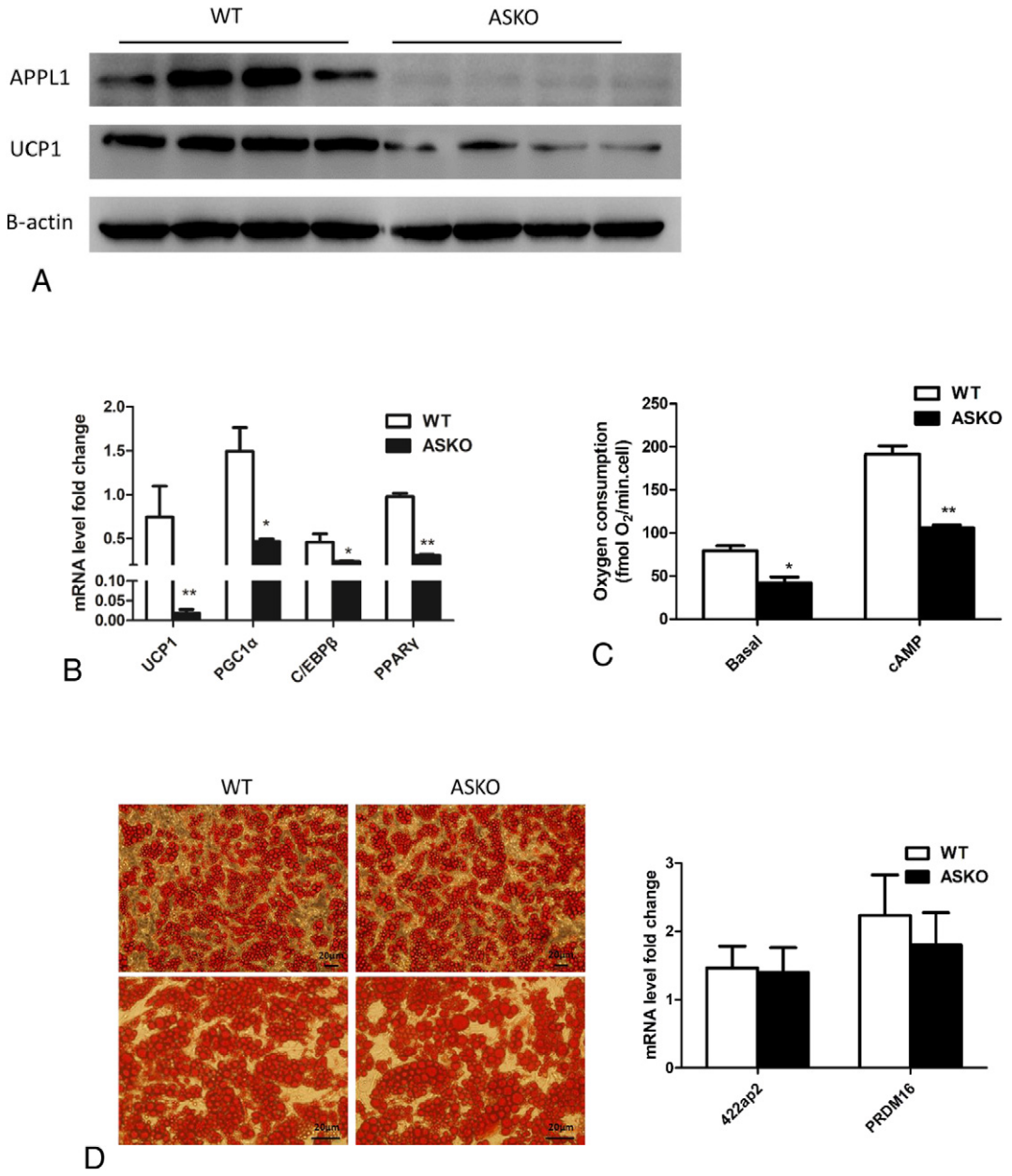

Fig. 5. APPL1 deficiency results in decreased thermogenic gene expressions in differentiated SVF from BAT. A: Western blot shows induction of UCP1 protein expression in differentiated SVF from 4-weeks-old WT and ASKO male mice. B: Real time qPCR analysis to quantify thermogenic gene expression levels. C. Oxygen consumption rate of the differentiated SVF brown adipocytes isolated from WT and ASKO mice. D. Oil red O staining for differentiated SVF brown adipocytes and differentiation-related genes expressions. ($n = 6$ per genotype) Data are represented as means ± SEM, and significant differences compared with controls are indicated by $^{*}P < 0.05$, $^{**}P < 0.01$.

predominantly in the nucleus [7]. Accumulating evidence has shown that class I HDAC inhibitor could induce thermogenic gene expression and alleviate obesity [9,10,36–39]. Previous study demonstrated that brown adipocytes treated with class I-specific HDAC inhibitor showed higher expression of PGC-1α, increased mitochondrial biogenesis, and augmented oxygen consumption [9]. Treatment of obese diabetic mice with a class I–selective HDAC inhibitor enhanced oxidative metabolism in skeletal muscle and adipose tissue and promoted energy expenditure, thus reducing body weight and glucose and insulin levels [36,37]. In vivo ChIP experiments indicated that inhibition of HDAC3 may account for the beneficial effect of the class I–selective HDAC inhibitor [9]. Specific ablation of HDAC3 in adipose tissue increased acetylation of enhancers in UCP1 genes which indicates that HDAC3 acts as a molecular brake of browning [39]. Our research in vitro indicates that in cAMP stimulation, APPL1 shuttled from cytosol to nuclei and directly interacted with HDAC3 to mediate chromatin remodeling and UCP1 gene expression in brown adipocytes (Fig. 6). However, other studies reported inconsistent results regarding adipocyte specific HDAC3 deletions [38,40]. Instead of inhibition by cold exposure, HDAC3 primes UCP1 in the acute thermogenesis in BAT in mice. After all, in this study, HDAC3 protein levels are decreased in brown fat after cold exposure, which are in agreement with our results. We have proved that after cold challenge, APPL1 expression was upregulated, adipose specific knockout APPL1 mice showed decreased BAT activity and impaired cold tolerance, APPL1 directly interacted with HDAC3 and its deletion resulted in loss inhibition of HDAC3. Concisely, in brown adipocytes, APPL1 is an endogenous HDAC inhibitor that could modulate thermogenic gene expression. Acetylation of histone 3 lysine 27 (H3K27ac) is known as a potent activation mark for browning-related genes, such as UCP1 [41,42]. H3K27ac distinguish active enhancers which favors transcriptional activation. Consistently, our results showed

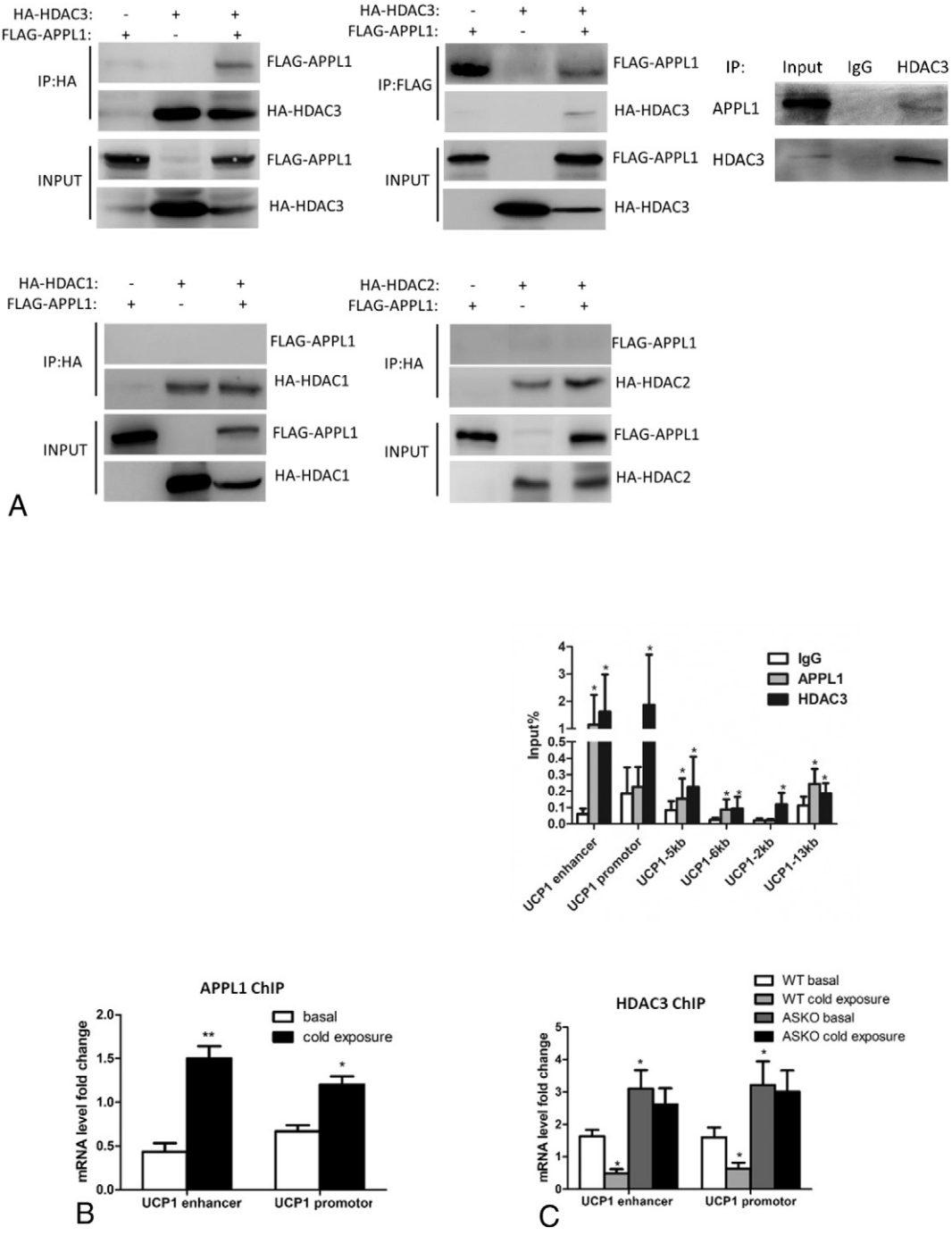

Fig. 6. APPL1 interacts with HDAC3 by nucleus shuttling to inhibit its function. A: Co-IP FLAG-APPL1 with HA-HDAC1/2/3 in HEK293T cells. B: After stimulation (cAMP) cell fractionation from brown adipocytes was performed by western blot analysis for APPL1, β-actin and Histone3 were examined as a positive control for cytosol and nuclear protein, respectively. C: BAT was collected for ChIP assay to measure APPL1 and HDAC3 binding to the enhancer and proximal promoter regions of UCP1 after cold exposure in both WT and ASKO mice (4 °C) ($n = 3$ per genotype). D. Over expressed APPL1 SVF, APPL1 knock out SVF and tissue fractionations directly derived from WT and ASKO mice all tested the acetylation level of H3K27 by western blot. Data are represented as means ± SEM, and significant differences compared with controls are indicated by $^{*}P < 0.05$ vs IgG or WT basal, $^{**}P < 0.01$ and $^{***}P < 0.001$.

that APPL1 overexpression increased the acetylation level of H3K27ac, while APPL1 deficiency conversely decreased the acetylation level (Fig. 6D). We propose that at basal condition, HDAC3 binding to the upstream promoter region of UCP1, deacetylates H3K27ac and inhibits gene expression. After cold challenge, APPL1 transfers to nuclei and inhibits the function of HDAC3, which increases acetylation of H3K27 to facilitate UCP1 gene expression.

In summary, our study demonstrated that APPL1 deficiency in adipose tissue caused male mice to be more susceptible to HFD-induced obesity, glucose intolerance, insulin resistance and BAT dysfunction. Our results suggest that APPL1 is integral to the BAT thermogenic response by interacting with HDAC3. These shed light on new sides of adipose tissue physiology that could be explored for new approaches related to metabolic disorders.

Author contributions

Yi Wang, Linling Fan, Yun Wan, Jing Su and Qiongyue Zhang conceived and designed the study and wrote the manuscript. Hongying Ye, Lang Qing, Lu Zhu, Xiaoming Zhu, Lv Zhang and Qing Miao

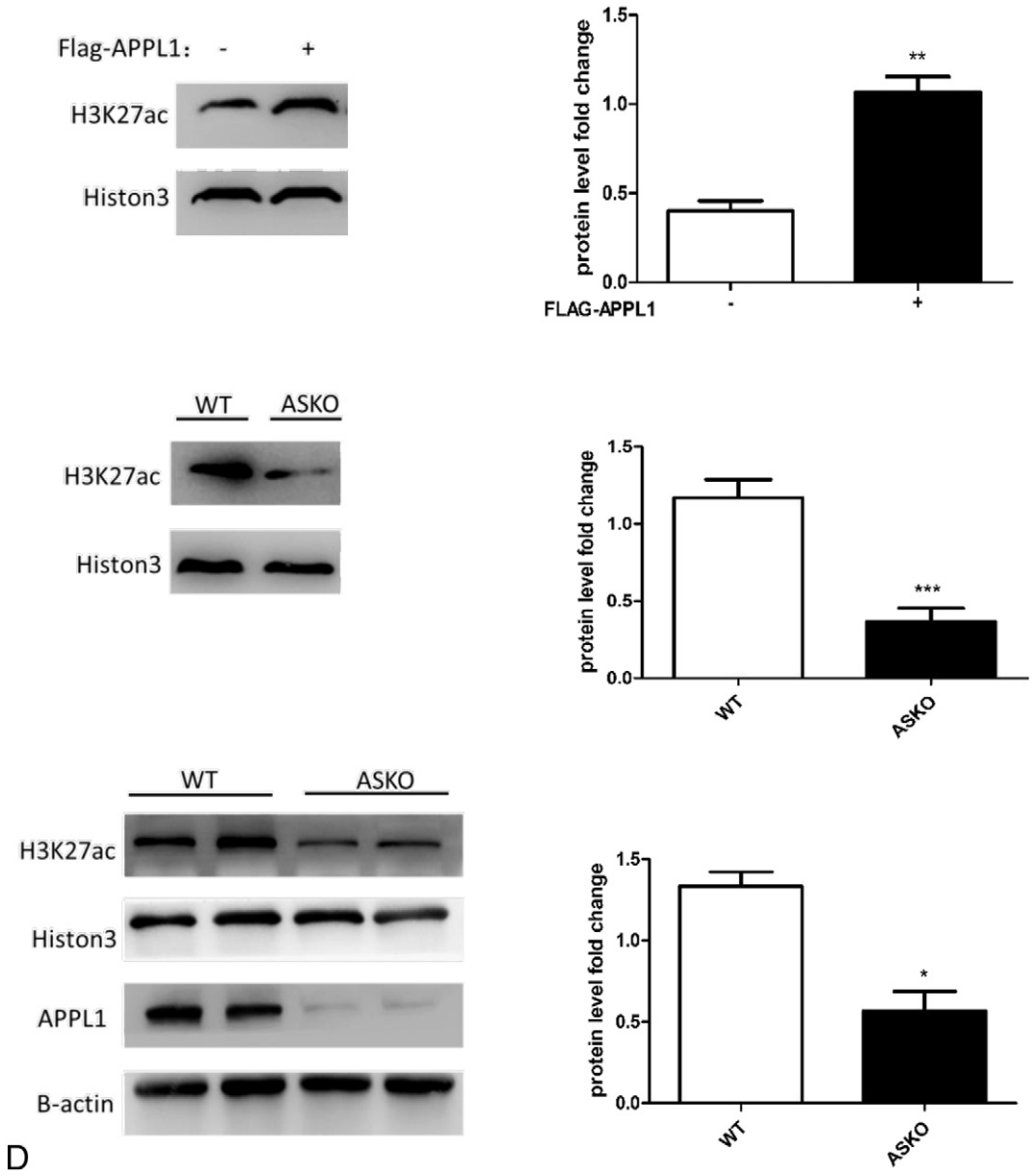

Fig. 6 (*continued*).

performed experiments and analyzed data. Zhaoyun Zhang, Aiming Xu, Yiming Li, Xi Li and Yi Wang assisted with experimental design and data interpretation.

Acknowledgement

This work was supported by National Natural Science Foundation of China (81400844 to Yi Wang, 81770861 and 31571401 to Xi Li, 81770840 to Yiming Li, 81800691 to Qing Miao), Shanghai Municipal Science and Technology Commission (17ZR1403900 to Hongying Ye), Shanghai Municipal Commission of Health and Family Planning Foundation (20164Y0041 to Qing Miao, 20144Y0070 to Qiongyue Zhang), Shanghai sailing program (19YF1404500 to Jing Su).

Declaration of competing interest

The authors declare no competing financial interests.

Appendix A. Supplementary data

Supplementary data to this article can be found online at https://doi.org/10.1016/j.metabol.2019.153955.

References

[1] Schwartz MW, Seeley RJ, Zeltser LM, Drewnowski A, Ravussin E, Redman LM, et al. Obesity pathogenesis: An Endocrine Society scientific statement. Endocr Rev 2017; 38:267–96.
[2] Lazar MA. Developmental biology. How now, brown fat? Science 2008;321:1048–9.
[3] McGlashon JM, Gorecki MC, Kozlowski AE, Thirnbeck CK, Markan KR, Leslie KL, et al. Central serotonergic neurons activate and recruit thermogenic brown and beige fat and regulate glucose and lipid homeostasis. Cell Metab 2015;21:692–705.
[4] Ruiz-Ojeda FJ, Ruperez AI, Gomez-Llorente C, Gil A, Aguilera CM, et al. Int J Mol Sci 2016;17.
[5] Rui L. Brown and beige adipose tissues in health and disease. Compr Physiol 2017;7: 1281–306.
[6] Sambeat A, Gulyaeva O, Dempersmier J, Sul HS. Epigenetic regulation of the thermogenic adipose program. Trends Endocrinol Metab 2017;28:19–31.

[7] de Ruijter AJ, van Gennip AH, Caron HN, Kemp S, van Kuilenburg AB. Histone deacetylases (HDACs): characterization of the classical HDAC family. Biochem J 2003;370:737–49.
[8] Yoo EJ, Chung JJ, Choe SS, Kim KH, Kim JB. Down-regulation of histone deacetylases stimulates adipocyte differentiation. J Biol Chem 2006;281:6608–15.
[9] Galmozzi A, Mitro N, Ferrari A, Gers E, Gilardi F, Godio C, et al. Inhibition of class I histone deacetylases unveils a mitochondrial signature and enhances oxidative metabolism in skeletal muscle and adipose tissue. Diabetes 2013;62:732–42.
[10] Li F, Wu R, Cui X, Zha L, Yu L, Shi H, et al. Histone deacetylase 1 (HDAC1) negatively regulates thermogenic program in brown adipocytes via coordinated regulation of histone H3 lysine 27 (H3K27) deacetylation and methylation. J Biol Chem 2016; 291:4523–36.
[11] Miaczynska M, Christoforidis S, Giner A, Shevchenko A, Uttenweiler-Joseph S, Habermann B, et al. APPL proteins link Rab5 to nuclear signal transduction via an endosomal compartment. Cell 2004;116:445–56.
[12] Li J, Mao X, Dong LQ, Liu F, Tong L. Crystal structures of the BAR-PH and PTB domains of human APPL1. Structure 2007;15:525–33.
[13] Mitsuuchi Y, Johnson SW, Sonoda G, Tanno S, Golemis EA, Testa JR. Identification of a chromosome 3p14.3–21.1 gene, APPL, encoding an adaptor molecule that interacts with the oncoprotein-serine/threonine kinase AKT2. Oncogene 1999;18:4891–8.
[14] Fang QC, Jia WP, Gao F, Zhang R, Hu C, Wang CR, et al. Association of variants in APPL1 gene with body fat and its distribution in Chinese patients with type 2 diabetic mellitus. Zhonghua Yi Xue Za Zhi 2008;88:369–73.
[15] Farias JM, Maggi RM, Tromm CB, Silva LA, Luciano TF, Marques SO, et al. Exercise training performed simultaneously to a high-fat diet reduces the degree of insulin resistance and improves adipoR1-2/APPL1 protein levels in mice. Lipids Health Dis 2012;11:134.
[16] Marinho R, Ropelle ER, Cintra DE, De Souza CT, Da SA, Bertoli FC, et al. Endurance exercise training increases APPL1 expression and improves insulin signaling in the hepatic tissue of diet-induced obese mice, independently of weight loss. J Cell Physiol 2012;227:2917–26.
[17] Schmid PM, Resch M, Steege A, Fredersdorf-Hahn S, Stoelcker B, Birner C, et al. Globular and full-length adiponectin induce NO-dependent vasodilation in resistance arteries of Zucker lean but not Zucker diabetic fatty rats. Am J Hypertens 2011;24: 270–7.
[18] Yan Y, An J, Yang Y, Wu D, Bai Y, Cao W, et al. Dual inhibition of AKT-mTOR and AR signaling by targeting HDAC3 in PTEN- or SPOP-mutated prostate cancer. EMBO Mol Med 2018;10.
[19] Joshi P, Greco TM, Guise AJ, Luo Y, Yu F, Nesvizhskii AI, et al. The functional interactome landscape of the human histone deacetylase family. Mol Syst Biol 2013;9:672.
[20] Tseng YH, Kokkotou E, Schulz TJ, Huang TL, Winnay JN, Taniguchi CM, et al. New role of bone morphogenetic protein 7 in brown adipogenesis and energy expenditure. Nature 2008;454:1000–4.
[21] Cheng KK, Iglesias MA, Lam KS, Wang Y, Sweeney G, Zhu W, et al. APPL1 potentiates insulin-mediated inhibition of hepatic glucose production and alleviates diabetes via Akt activation in mice. Cell Metab 2009;9:417–27.
[22] Saito T, Jones CC, Huang S, Czech MP, Pilch PF. The interaction of Akt with APPL1 is required for insulin-stimulated Glut4 translocation. J Biol Chem 2007;282:32280–7.
[23] Mao X, Kikani CK, Riojas RA, Langlais P, Wang L, Ramos FJ, et al. APPL1 binds to adiponectin receptors and mediates adiponectin signalling and function. Nat Cell Biol 2006;8:516–23.
[24] Ryu J, Galan AK, Xin X, Dong F, Abdul-Ghani MA, Zhou L, et al. APPL1 potentiates insulin sensitivity by facilitating the binding of IRS1/2 to the insulin receptor. Cell Rep 2014;7:1227–38.
[25] Wang Y, Cheng KK, Lam KS, Wu D, Wang Y, Huang Y, et al. APPL1 counteracts obesity-induced vascular insulin resistance and endothelial dysfunction by modulating the endothelial production of nitric oxide and endothelin-1 in mice. Diabetes 2011;60:3044–54.
[26] Lee KY, Russell SJ, Ussar S, Boucher J, Vernochet C, Mori MA, et al. Lessons on conditional gene targeting in mouse adipose tissue. Diabetes 2013;62:864–74.
[27] Garcia-Martin R, Alexaki VI, Qin N, Rubin DCM, Economopoulou M, Ziogas A, et al. Adipocyte-specific hypoxia-inducible factor 2alpha deficiency exacerbates obesity-induced brown adipose tissue dysfunction and metabolic dysregulation. Mol Cell Biol 2016;36:376–93.
[28] Kontani Y, Wang Y, Kimura K, Inokuma KI, Saito M, Suzuki-Miura T, et al. UCP1 deficiency increases susceptibility to diet-induced obesity with age. Aging Cell 2005;4: 147–55.
[29] Feldmann HM, Golozoubova V, Cannon B, Nedergaard J. UCP1 ablation induces obesity and abolishes diet-induced thermogenesis in mice exempt from thermal stress by living at thermoneutrality. Cell Metab 2009;9:203–9.
[30] Stanford KI, Middelbeek RJ, Townsend KL, An D, Nygaard EB, Hitchcox KM, et al. Brown adipose tissue regulates glucose homeostasis and insulin sensitivity. J Clin Invest 2013;123:215–23.
[31] Orava J, Nuutila P, Noponen T, Parkkola R, Viljanen T, Enerback S, et al. Blunted metabolic responses to cold and insulin stimulation in brown adipose tissue of obese humans. Obesity (Silver Spring) 2013;21:2279–87.
[32] Brendle C, Werner MK, Schmadl M, la Fougere C, Nikolaou K, Stefan N, et al. Correlation of brown adipose tissue with other body fat compartments and patient characteristics: a retrospective analysis in a large patient cohort using PET/CT. Acad Radiol 2018;25:102–10.
[33] Banach-Orlowska M, Pilecka I, Torun A, Pyrzynska B, Miaczynska M. Functional characterization of the interactions between endosomal adaptor protein APPL1 and the NuRD co-repressor complex. Biochem J 2009;423:389–400.
[34] Rashid S, Pilecka I, Torun A, Olchowik M, Bielinska B, Miaczynska M. Endosomal adaptor proteins APPL1 and APPL2 are novel activators of beta-catenin/TCF-mediated transcription. J Biol Chem 2009;284:18115–28.
[35] Song J, Mu Y, Li C, Bergh A, Miaczynska M, Heldin CH, et al. APPL proteins promote TGFbeta-induced nuclear transport of the TGFbeta type I receptor intracellular domain. Oncotarget 2016;7:279–92.
[36] Ferrari A, Fiorino E, Longo R, Barilla S, Mitro N, Cermenati G, et al. Attenuation of diet-induced obesity and induction of white fat browning with a chemical inhibitor of histone deacetylases. Int J Obes (Lond) 2017;41:289–98.
[37] Rajan A, Shi H, Xue B. Class I and II histone deacetylase inhibitors differentially regulate thermogenic gene expression in brown adipocytes. Sci Rep 2018;8:13072.
[38] Liao J, Jiang J, Jun H, Qiao X, Emont MP, Kim DI, et al. HDAC3-selective inhibition activates brown and beige fat through PRDM16. Endocrinology 2018;159:2520–7.
[39] Ferrari A, Longo R, Fiorino E, Silva R, Mitro N, Cermenati G, et al. HDAC3 is a molecular brake of the metabolic switch supporting white adipose tissue browning. Nat Commun 2017;8:93.
[40] Emmett MJ, Lim HW, Jager J, Richter HJ, Adlanmerini M, Peed LC, et al. Histone deacetylase 3 prepares brown adipose tissue for acute thermogenic challenge. Nature 2017;546:544–8.
[41] Chatterjee TK, Basford JE, Knoll E, Tong WS, Blanco V, Blomkalns AL, et al. HDAC9 knockout mice are protected from adipose tissue dysfunction and systemic metabolic disease during high-fat feeding. Diabetes 2014;63:176–87.
[42] Yuliana A, Jheng HF, Kawarasaki S, Nomura W, Takahashi H, Ara T, et al. beta-adrenergic receptor stimulation revealed a novel regulatory pathway via suppressing histone deacetylase 3 to induce uncoupling protein 1 expression in mice beige adipocyte. Int J Mol Sci 2018;19.